Journal of Alloys and Compounds 912 (2022) 165233

Contents lists available at ScienceDirect

Journal of Alloys and Compounds

journal homepage: www.elsevier.com/locate/jalcom

Synthesis and spark plasma sintering of solid-state matrices based on calcium silicate for ^{60}Co immobilization

O.O. Shichalin[a,*], S.B. Yarusova[b,c], A.I. Ivanets[d], E.K. Papynov[a], A.A. Belov[a], S.A. Azon[a], I. Yu Buravlev[a,b], A.E. Panasenko[b], P.A. Zadorozhny[b], V.Yu Mayorov[a,b], D. Kh Shlyk[b], V.A. Nepomnyushchaya[a], O.V. Kapustina[a], A.E. Ivanova[a], A.A. Buravleva[a], E.B. Merkulov[b], P.S. Gordienko[b]

[a] Far Eastern Federal University, 10 Ajax Bay, Russky Island, Vladivostok 690922, Russia
[b] Institute of Chemistry, Far Eastern Branch of Russian Academy of Sciences, 159, Prosp. 100-letiya Vladivostoka, Vladivostok 690022, Russia
[c] Vladivostok State University of Economics and Service, Gogolya st., 41, Vladivostok 690014, Russia
[d] Institute of General and Inorganic Chemistry of National Academy of Sciences of Belarus, Surganova st. 9/1, Minsk 220072, Belarus

ARTICLE INFO

Article history:
Received 26 March 2022
Received in revised form 18 April 2022
Accepted 26 April 2022
Available online 30 April 2022

Keywords:
Calcium silicate
Co^{2+} adsorption
Spark plasma sintering
Silicate matrices
^{60}Co immobilization

ABSTRACT

An effective sorption material for the immobilization of cobalt radionuclides into highly safe and reliable solid-state matrices is proposed. The resulting silicate sorbent $CaSiO_3$ had an amorphous mesoporous structure (A_{BET} 53 m^2/g) and a sorption capacity Co ions of 3.32 mmol/g. The physico-chemical characteristics of the $CaCoSi_2O_6$ sample obtained after Co^{2+} ions sorption were studied using XRD, N_2 and Ar adsorption-desorption, SEM-EDX and TG/DTA methods. Solid-state silicate matrices characterized by high density values (2.86–3.16 g/cm^3), compressive strength (150–637 MPa) and Vickers microhardness (1.80–5.25 GPa) were obtained by spark plasma sintering (SPS). The sample obtained at 1000 °C had the lowest values of Co^{2+} ions leaching (R_{Co} ~10^{-7} $g/(cm^2 \times day)$) and diffusion coefficient (De 1.73 ×10^{-17} cm^2/s) from silicate matrices. Thus, the obtained $CaCoSi_2O_6$ silicate matrices saturated with Co ions comply with the regulatory requirements of GOST R 50926–96 and ANSI/ANS 16.1 for ^{60}Co immobilization.

1. Introduction

Among all artificial radioactive isotopes, ^{60}Co with a half-life of about 5 years has found wide application. The search for promising materials for the sorption and ^{60}Co immobilization, which is a source of gamma radiation, is an urgent task in the context of radioactive waste management [1]. A wide range of inorganic and organic materials are used for cobalt sorption: polymers, modified resins [2–5], phosphates of multivalent metals of various compositions (Ca-Mg-PO_4, Ti-Ca-Mg-PO_4) [6,7], magnetite nanoparticles[8], composite sorbents based on magnetite and zeolite [9], goethite [10], aluminum oxide γ-Al2O3 [11], derivatives of inosithexaphosphoric acid [12], biosorbents [13,14]. The sorption capacity of the studied sorbents varies from units to 500 mg/g, depending on the experimental conditions. Cobalt has 37 radioisotopes with mass numbers from 47 to 75. ^{59}Co is the only stable isotope. The isotopes ^{57}Co, ^{58}Co and ^{60}Co are the most widely produced, of which only ^{60}Co has a half-life of more than a year (Table 1) [15].

For the management of solid and liquid radioactive waste containing beta-gamma emitters, mainly ^{134,137}Cs, ^{90}Sr, ^{60}Co and impurities of alpha-emitting radionuclides of complex chemical composition, high-temperature matrices with high chemical and radiation resistance, as well as mechanical strength are promising [16–18]. At the same time, among the inorganic ceramic materials used for the nuclear waste immobilization, special attention is paid to the consideration of silicates of various composition and structure, which is confirmed by a recent review [19]. A number of works are devoted to the study of cobalt removal from aqueous media by silicate sorbents. The authors [20] studied the sorption of long-lived radionuclides of cesium, strontium and cobalt (^{134}Cs, ^{85}Sr and ^{60}Co) on bentonite $Al_2[Si_4O_{10}](OH)_2 \cdot nH_2O$ under various experimental conditions (contact time, pH, sorbent and sorbate concentrations). The ^{134}Cs and ^{85}Sr sorption occurred rapidly, and equilibrium was achieved almost instantly in both cases, while the sorption kinetics of ^{60}Co was significantly lower. Sorption of the studied radionuclides increased with an increase in pH and with an increase in the amount

* Corresponding author.
E-mail address: oleg_shich@mail.ru (O.O. Shichalin).

https://doi.org/10.1016/j.jallcom.2022.165233
0925-8388/

Table 1
Physical characteristics of ^{60}Co isotope.

Parameters	^{60}Co
Radioactive half-life	5.27 years
Specific activity	4.19×10^{13} Bq·g^{-1}
Precursors	$^{60\ m}Co$ (from ^{60}Fe)
Decay product	^{60}Ni
Principal emission through disintegration (emission probability, %)	β - 318 keV (99.9%) γ 1.332 keV (100%) and 1.173 keV (99.9%)

of bentonite clay. The ^{134}Cs, ^{85}Sr and ^{60}Co removal efficiency decreased with an increase in the metal ions concentration. Desorption studies with 0.01 M $CaCl_2$ and ground water at low concentrations of metal ions on bentonite showed that about 95% of ^{134}Cs, 85–90% ^{85}Sr and 97% ^{60}Co were irreversibly sorbed. These results can be useful for the processing of nuclear waste and wastewater containing low concentrations of cesium, strontium and cobalt ions.

Sorption properties of natural and synthetic allophane aluminosilicate Al_2O_3 $(SiO_2)_{1-2}(H_2O)_{5-6}$, which is a natural clay mineral widely distributed in volcanic ash layers and soils, were studied [21]. The specific surface area of the studied samples was 294–370 m^2/g. Sorption was carried out in the concentration range of 1–100 mg/L for 2 h at a temperature of 25 °C and pH 8.5. The highest values of sorption capacity for cobalt ions were observed in synthetic allophanes and reached 29 mg/g.

The authors [22] studied the properties of kaolinite and montmorillonite with a specific surface area of 3.8 and 19.8 m^2/g in the concentration range of 10–250 mg/L for 240 min at a temperature of 30 °C and pH 5.8. The maximum sorption capacity was 11.0 for kaolinite and 28.6 mg/g for montmorillonite. Natural bentonite, zeolite and their mixture were studied during cobalt sorption [23] in the concentration range of 5–50 mg/L for 1–12 h. The determined monolayer Langmuir sorption capacity was 2.73 mg/g. Among the silicates used for cobalt removal, calcium silicates and aluminosilicates are mostly studied [24–32].

In the study [24], gels based on calcium and aluminum silicate hydrate (CASH) containing heavy metal ions (Co^{2+}, Cu^{2+} and Zn^{2+}) were precipitated at various M/Si molar ratios to study the mechanism of sorption and immobilization capacity. The threshold value for ion substitution is ~ 30–40 mol.% for Co^{2+} in defective CASH tobermorite type with molar ratios (Ca+M)/(Si+Al) from 0.86 to 1.04. The sorption properties of hydrated aluminosilicates synthesized by the sol-gel method at different initial molar ratios of Ca/(Si + Al)$_{(0.6-1.6)}$ and M/Si$_{(0.0-2.0)}$ and a constant ratio of Al/Si (0.05) were studied [25]. The sorption capacity of hydrated calcium aluminosilicates to cobalt ions reached 40 mg/g. The mechanism of heavy metals immobilization was based on a combination of isomorphic substitution, interlayer cation exchange, adsorption and surface deposition. The sorbent based on 11 Å tobermorite obtained from the remnants of newsprint recycling was characterized by a low sorption capacity of 10.47 mg/g (or 0.177 mmol/g) cobalt ions from acidic solutions at a ratio of solid and liquid phases S:L = 1:20 and a temperature of 20 °C [26]. Thus, in engineering systems, such as underground concrete structures and nuclear waste disposal sites, hydrated aluminosilicates should demonstrate high efficiency of heavy metal ion retention.

The ion-exchange capacity of Co^{2+} ions calculated in [26] for calcium-silicate sorbents of xonotlite and wollastonite obtained from synthetic and natural components was 0.2–0.5 and 0.25–0.4 mmol/g at S:L = 1:250, pH 8 and temperature 25 °C. The sorption characteristics of calcium silicates obtained in a multicomponent $CaCl_2$ – Na_2SiO_3 – H_2O system and from boric acid production waste were studied. The maximum sorption capacity to Co^{2+} ions reached 4.0 mmol/g [29,30]. Advantages of SPS is the subject of close attention of scientists with the purpose of its use in radiochemical production for the creation of solid-state matrices with immobilized radionuclides. High-speed heating of radioactive charge and a short sintering time at relatively low temperatures and the formation of dense amorphous or crystalline compacts with a given microstructure and composition ensure strong binding of radionuclides, which is an exceptional technological feature of the SPS. It is due to the reduced stages of charge fractionation, elimination of the introduction of binder additives, increased accuracy of batching of products by specific activity, obtaining products of small shapes and sizes with high-performance characteristics.[33–36]. In addition, using SPS technology, it is possible to produce radionuclide products[37,38]. Spark plasma sintering-reactive synthesis method (SPS-RS) is a technology of high progress. This method is based on the in situ solid-phase reaction of powder mixtures under conditions of spark plasma heating. Method for determining the high rate of formation of a desired compound while introducing it into a dense ceramic mixture[39–41].

The relatively low capacity of silicates and aluminosilicate sorbents to Co^{2+} ions, as well as kinetic limitations, are the main drawbacks limiting the widespread use of this materials. Thereof, it seems relevant to obtain amorphous hydrated calcium silicate in the above-mentioned multicomponent system and solid-state matrices based on it for reliable cobalt radionuclides immobilization using spark plasma sintering (SPS) technology.

2. Experimental

2.1. Chemicals

Sodium metasilicate Na_2SiO_3·5 H_2O (99.9%, Sigma-Aldrich), Calcium chloride $CaCl_2$·2 H_2O (99.9%, Sigma-Aldrich), Cobalt chloride $CoCl_2$·6H_2O (99.99%, Sigma-Aldrich) reagents without additional purification were used.

2.2. Synthesis of $CaSiO_3$ sorbent

The synthesis of hydrated calcium silicate was carried out in the $CaCl_2$ – Na_2SiO_3 – H_2O system. Sodium silicate (liquid glass) with SiO_2/Na_2O molar ratio of 1.0 and calcium chloride dihydrate $CaCl_2$.2 H_2O were used as initial reagents. The chemicals were mixed in an aqueous medium in chemical flasks, as described in [29]. The resulting precipitate was washed with distilled water, filtered through a blue ribbon filter and dried at 85 °C.

2.3. Sorption characteristics of $CaSiO_3$ sorbent

The resulting precipitate, pre-dried to a constant weight at a temperature of 105 °C, was treated under static conditions with an aqueous solution of cobalt chloride $CoCl_2$·6H_2O with Co^{2+} concentration of 110.1 mmol/L until it was completely saturated, with a ratio of solid and liquid phases S:L equal to 1:40, and a temperature of 20 °C for 24 h with stirring at 150 rpm on a magnetic stirrer RT 15 power (IKA WERKE, Germany). Then the solution was separated from the sorbent by filtration through a blue ribbon filter using a water jet pump and the concentration of Co^{2+} and Ca^{2+} ions in the filtrate was determined. The precipitate was thoroughly washed with hot distilled water until the negative reaction of the washing solution to Cl^--ions. The sorption capacity for Co^{2+} ions under these conditions was 3.32 mmol/g, which corresponds to the cobalt content in the saturated sample of 37.2 wt%.

2.4. Spark plasma sintering of $CaCoSi_2O_6$ solid-state matrices

SPS synthetic $CaCoSi_2O_6$ matrices was conducted on a LABOX-625 (Japan) instrument. Saturated calcium silicate sorbent was put into cylindrical graphite die (outer diameter of 30 mm, internal diameter

of 15.3 mm, height of 30 mm), prepressed at 20.7 MPa, further the green tablet was transferred into a vacuum chamber (6 Pa) and sintered. Temperature measurement is performed by Hitachi IR-AHS pyrometer (600–3000 °C). Heating was conducted by the pulse current in the On/Off regime with the periodicity of the pulse/pause of 12/2 (39.6/6.6 ms). Calcination temperature was 800, 900, 1000 °C, heating rate of 100 °C/min, holding time at final temperature and cooling time were 5 and 30 min, respectively. The uniaxial pressure load during sintering was maintained constant at 24.5 MPa. The obtained samples were cylindrical shape with a diameter of 15.3 mm and height of 4–6 mm.

2.5. Characterization methods

XRD was carried out on a "D8 Advance Bruker AXS" (Germany) diffractometer. Particle size distribution was determined on a particle size analyzer Analysette-22 NanoTec/MicroTec/XT "Fritsch" (Germany). The thermogravimetric curves were recorded on the STA 449 C NETZSCH device in platinum crucibles with a pierced lid in a dry argon stream (20 mL/min) in the temperature range of 35–1300 °C and the heating rate of 10 °C/min. The weight of the attachments was about 40 mg, weighing was carried out on Sartorius CP2P micro weights with an accuracy of 1 μg. Scanning electron microscopy (SEM) was done on a CrossBeam 1540 XB "Carl Zeiss" (Germany) equipped with the add-on for energy dispersive X-Ray spectral analysis (EDX) "Bruker" (Germany). The content of carbonates (in terms of dry weight) was quantified by a gas-volume method based on measuring the volume of gas extracted from the solid weight. Specific area was measured using an analyzer of low-temperature N_2 and Ar adsorption-desorption at 77 K (Autosorb IQ, "Quantochrome", USA). The BET, SF, HK models was used for the texture characteristics calculations. Compressive strength (σcs.) was evaluated on a tensile machine Autograph AG-X plus 100 kN "Shimadzu" (Japan).

Vickers microhardness (HV) was determined at 0.2 N load on a microhardness tester HMV-G-FA-D "Shimadzu" (Japan). Experimental density (ED) was measured by hydrostatic weighing on the balance Adventurer™ "OHAUS Corporation" (USA). Relative density (RD) was found as a ratio of the experimental density (ED) measured via hydrostatic weighing to the theoretical density (TD).

2.6. Evaluation of metal ions leaching from $CaCoSi_2O_6$ silicate matrices

Metal ions leaching from silicate matrices was estimated based on leaching rate of cobalt and calcium ions under 30 days contact with the distilled water (pH 6.8) at room temperature (25 °C) in static condition according to well-known Russian Government Standard (GOST R 52126–2003), closely related to the ANSI/ANS-American National Standards Institute/American Nuclear Society 2019 (ANSI/ANS 16.1) that was updated according to the older procedure recommended by IAEA (ISO 6961:1982). Cobalt concentration was found on an atomic absorption spectrometer SOLAAR M6 "Thermo Scientific" (USA).

The calculation of the effective diffusion coefficient (D_e) was performed by mathematical transformations of the second Fick law according to the method described in [42]:

$$\frac{\sum m}{M_0} = 2\left(\frac{D_e}{\pi}\right)^{\frac{1}{2}}\left(\frac{S}{V}\right)t^{\frac{1}{2}} + \alpha \quad (1)$$

where is m – cesium weight, mg, leaching ta time t, s, M_0 – initial cesium content in the sample, mg, D_e – effective diffusion coefficient, cm^2/s, S – the surface area of the sample, cm^2, V – a volume of sample, cm^3, α – parameter that takes into account the initial leaching of cesium, not related to diffusion (cesium leaches out at the initial contact of the leaching solution with the sample surface).

To calculate this equation was reduced to a linear form by introducing the coefficient K, which is the tangent of the slope angle of the direct dependence of the cesium fraction leached from the sample on the square root of the contact time of the material with the leaching agent:

$$K = 2\left(\frac{D_e}{\pi}\right)^{0,5}\cdot\left(\frac{S}{V}\right) \quad (2)$$

The effective diffusion coefficient was calculated according to Eq. (3):

$$D_e = \frac{K^2\cdot\pi}{4}\cdot\left(\frac{V}{S}\right)^2 \quad (3)$$

The leaching index (L) was calculated as the decimal logarithm of the inverse diffusion value.

$$L = \lg\frac{1}{D_e} \quad (4)$$

Evaluation of the dominant leaching mechanism based on the dependence of the decimal logarithm of the accumulated fraction of leached radionuclide (B_t, mg/m^2) on the decimal logarithm of the leaching time t, s:

$$lg\quad(B_t) = \frac{1}{2}\lg t + lg\left[U_{max}d\sqrt{\frac{D_e}{\pi}}\right] \quad (5)$$

where is U_{max} – the maximum amount of leached radionuclide, mg/kg, d – matrix density, kg/m^3.

The leaching depth of the matrix characterizes the destruction of the matrix as a whole when it is in an aqueous medium. Eq. (6) calculated this characteristic:

$$L_i^i = \sum_1^n\left(W_n^i\cdot\frac{t_n}{d}\right) \quad (6)$$

where is L_i^i – the leaching depth of the matrix reached during the time interval t_n, cm, d – density of the sample, g/cm^3.

The error of the leaching rate is determined by the error of determining the concentration of the corresponding ions in the solution by the AAC method (no more than 15%). In addition, according to the works [42,43], the dominant metal ions leaching mechanism was evaluated.

3. Results and discussion

3.1. Characterization of $CaSiO_3$ adsorbent and $CaCoSi_2O_6$ solid-state matrices

According to X-ray diffraction analysis (XRD), the resulting precipitate contains calcium carbonate $CaCO_3$ in addition to the amorphous phase. This was due to the interaction of the reaction system with water vapor and the CO_2 adsorption from the air. The resulting calcium silicate partially decomposed to form $CaCO_3$ and amorphous silica, which was confirmed by previous studies and corresponding calculations [44–46]. It was found that the content of $CaCO_3$ was about 30%. Most of the works are devoted to high-temperature solid sorbents, such as CaO-based sorbents and alkaline ceramic sorbents [47]. Among these sorbents, lithium-based ceramics such as Li_2CuO_2, Li_5AlO_4, $LiFeO_2$, Li_2ZrO_3, Li_4TiO_4, Li_8SiO_6 and Li_4SiO_4 [48] are capable of efficiently CO_2 capturing at high temperature. At the same time, Li_4SiO_4 has the highest CO_2 sorption capacity (theoretically up to 367 mg/g), cyclic stability, as well as lower regeneration temperatures [48,49]. Thus, the prepared sorbent was a composite of amorphous calcium silicate, calcium carbonate and amorphous silica.

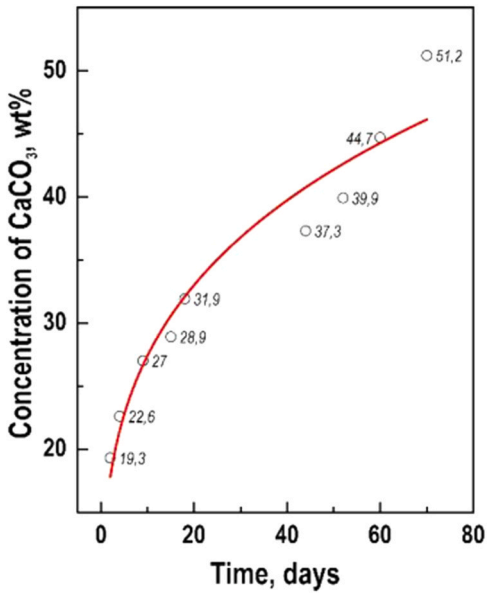

Fig. 1. Calcium carbonate content (wt%) depending on the exposure time of amorphous calcium silicate in air at 100% humidity.

The stability of the obtained sorbent to the influence of hydration processes and exposure to CO_2 in the air at 100% humidity was studied. The duration of the experiment ranged from 60 to 120 days. Fig. 1 shows the kinetics of the formation of calcium carbonate in a sample of the studied calcium silicate exposed under the above mentioned conditions. Thus, with an increase in the duration of exposure of hydrated calcium silicate in air in a humid atmosphere, the content of $CaCO_3$ in the sample increased, reaching 50% after 65 days. At the same time, the proportion of hygroscopic moisture in the sample also increased. The relative humidity of the initial sample and after exposure in a humid atmosphere with air accessed for 65 days was 3.13% and 16.81%, respectively. It should be noted that after holding the sample in a humid atmosphere with air access for 120 days, there was a decrease in the specific surface area and an increased in apparent density. This was due to the formation of calcium carbonate in the form of polymorphic modifications - calcite and aragonite. At the same time, aragonite has a higher density (2.94 g/cm^3) compared to calcite (2.72 g/cm^3).

The granulometric composition of the initial ($CaSiO_3$) and saturated with Co^{2+} ions ($CaCoSi_2O_6$) sorbents was represented by a wide fraction of particles with a size of 0.1–60 μm (Fig. 2a, b). The smallest fraction was < 1 μm, the average fraction was 1–10 μm in the form of agglomerates of smaller particles and the large fraction was represented by particles ranging in size from 20 to 60 μm. Thus, fractions 1–10 and 20–60 μm make the main contribution to the particle size distribution for the sorbent saturated with Co^{2+} ($CaCoSi_2O_6$) ions and contained more than 60% (Fig. 2b).

The results of the thermogravimetric study of the initial ($CaSiO_3$) and saturated with Co^{2+} ions ($CaCoSi_2O_6$) sorbents are shown in (Fig. 2c). It was shown that the content of physically bounded water (evaporated up to 200 °C) in the saturated sorbent was about 8%, which is twice as much as in the initial sorbent. The obtained amorphous calcium silicate, partially reacted with water and carbon dioxide contained in the atmosphere during storage: $CaO{\cdot}SiO_2{\cdot}nH_2O + CO_2 \rightarrow CaCO_3 + SiO_2{\cdot}nH_2O$, which was confirmed by XRD data. Therefore, the decomposition of the initial sample above 500 °C was primarily due to the $SiO_2{\cdot}nH_2O$ dehydration. Above 655 °C for the initial and at 720 °C for saturated samples, the decomposition of calcium carbonate occurred [50], which was indicated on the DTA curves by the endothermic effect and by dramatic weight losses on the TG curves. Further, for the initial sample at 845 °C, an exothermic effect was observed without weight loss due to wollastonite crystallization. For a saturated sorbent, a strongly expanded exothermic effect was also observed with a maximum at 1004 °C. The total weight loss in the studied temperature range was 28% for the initial and 27% for sorbents saturated with Co^{2+} ions. The sorption isotherm belongs to the C-type according to the Giles classification without a pronounced exit to the asymptotic plateau, which indicates that the sorbent saturation has not been achieved. The maximum sorption capacity of Co^{2+} ions of the obtained sorbent under the studied conditions was 3.32 mmol/g (Fig. 3). For a comparative assessment of the sorbent efficiency, the sorption capacities of silicates and aluminosilicates are given (Table 2). Thus, the prepared calcium silicate had enhanced sorption capacity compared to natural, synthetic and modified aluminosilicate and silicate adsorbents.

According to the SEM data, the sorbent saturated with Co^{2+} (CaCoSi2O6) was represented by spherical-like agglomerates of various sizes - from fine < 0.1 μm to coarse particles of 60–100 μm (Fig. 4a). This is in good agreement with the particle size distribution data (Fig. 2b). Coarse-dispersed agglomerates had a spongy structure (Fig. 4b, c), represented by rod-shaped particles 100–200 nm long and 20 nm thick (Fig. 4d).

To analysis changes in the adsorption and textural characteristics of the sorbent during Co^{2+} sorption, low-temperature adsorption-desorption of nitrogen of the initial (CaSiO3) and saturated with Co^{2+} ions ($CaCoSi_2O_6$) sorbents was carried out. Nitrogen adsorption - desorption isotherms for all samples had a hysteresis loop of

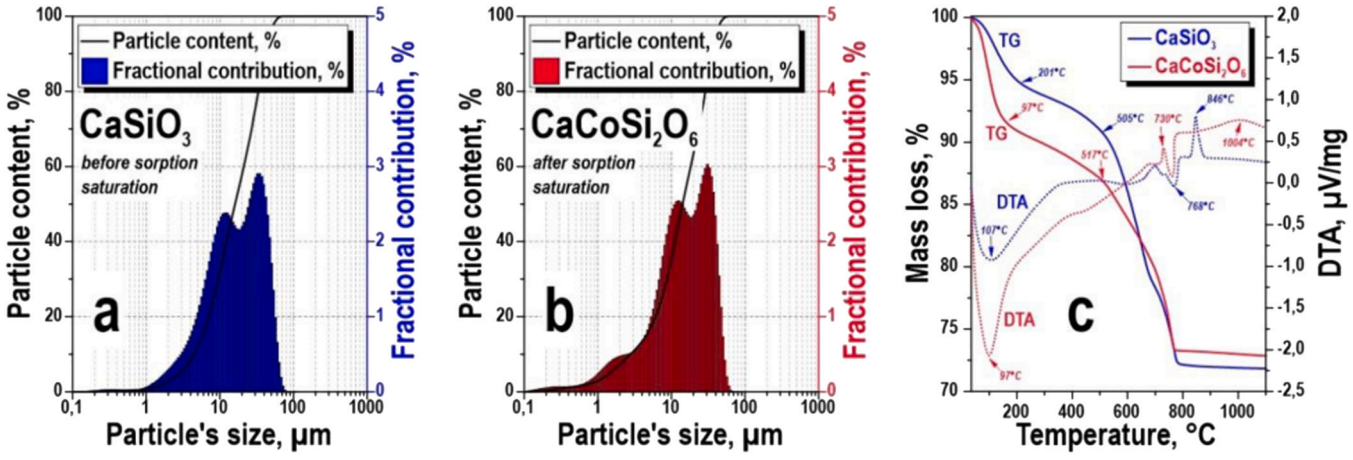

Fig. 2. (a, b) The particle size distribution and (c) TG/DTA curves of the initial ($CaSiO_3$) and saturated with Co^{2+} ions ($CaCoSi_2O_6$) sorbents.

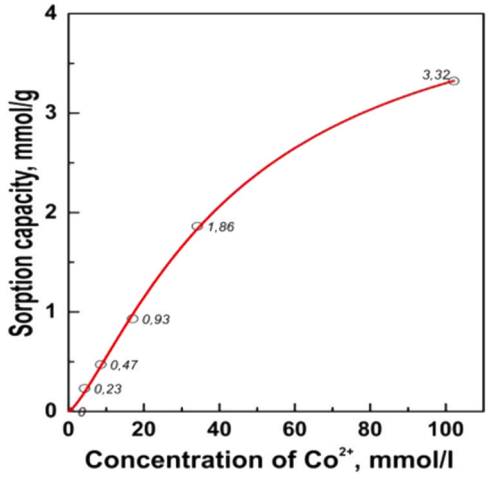

Fig. 3. Isotherm of Co^{2+} sorption on the prepared $CaSiO_3$ sorbent.

capillary condensation and belong to type IV according to the IUPAC classification, characteristic of mesoporous materials [60]. It should be noted that the nitrogen adsorption isotherm for the $CaCoSi_2O_6$ sample had a sharp vertical initial section, which indicates the presence of micropores in the structure.(Dummy Fig. 5).

The isotherms of the initial sorbent and after sorption of Co^{2+} ions did not have a saturation limit at p/p_0 ~ 1.0. This complicated the reliable determination of the pore size of > 100 nm. For the initial calcium silicate, the hysteresis loop had a clear H3 type, which indicated the presence of slit-like pores, which is also characteristic of materials with a layered structure. The DFT method can be used for the most correct calculation of the pore size distribution. The initial sorbent was characterized by a polymodal pore size distribution without a pronounced predominant pore radius in the range of 2–50 and 50–75 nm. After Co^{2+} ions sorption, the hysteresis loop type had a hybrid form of H2 +H3, which caused an artifact on the pore size distribution curve at 4 nm. Therefore, for a more correct construction of the pore size distribution, the desorption branch of the adsorption-nitrogen desorption isotherm was used. For the $CaCoSi_2O_6$ sample, a narrower pore size distribution wa s observed with a predominant radius in the mesopore region of 1.3–5.8 nm.

In addition to the above-described differences in nitrogen adsorption-desorption isotherms and pore size distributions calculated on their basis, the initial ($CaSiO_3$) and Co^{2+} ion-saturated ($CaCoSi_2O_6$) sorbents differed significantly in terms of specific surface area and pore volume. Thus, the specific surface A_{BET} of the initial $CaSiO_3$ sample was 55.8 m^2/g, and after saturation with Co^{2+} ions, the $CaCoSi_2O_6$ sample was 318 m^2/g. As a result of sorption, a slight change in pore volume was observed from 0.37 to 0.32 cm^3/g for the initial and saturated samples, respectively. The formation of micropores for $CaCoSi_2O_6$ sample was observed, as supported by the vertical initial section of the adsorption isotherm.

Analysis of changes in the adsorption and textural characteristics of $CaSiO_3$ and $CaCoSi_2O_6$ samples indicated the chemisorption mechanism of the Co^{2+} ions sorption on $CaSiO_3$ sorbent. The resulting highly dispersed $CaCoSi_2O_6$ phase was significantly differed in terms of adsorption and textural characteristics, which may be due to the Co^{2+} ions sorption by the dissolution-precipitation mechanism.

For a more detailed study of the structural changes of the sorbent during the Co^{2+} ions sorption, the Ar adsorption-desorption isotherms were measured (Fig. 6), as a sorbate with a smaller molecule size compared to nitrogen. Thus, the form of the Ar adsorption-desorption isotherm differed significantly from the isotherm obtained for nitrogen. In fact, the hysteresis loop disappears and the initial section of the isotherm had a pronounced vertical section, which is characteristic of type I isotherms according to the IUPAC classification, characteristic of micro/macroporous adsorbents (Fig. 6a). For a sorbent saturated with Co^{2+} ions, the initial section of the isotherm did not change compared to the nitrogen isotherm, while the section at p/p0 > 0.4 was significantly transformed. Thus, at high Ar relative pressures, the isotherm reached a plateau, and the hysteresis loop had the H1 shape characteristic of cylindrical pores. The obtained data on the Ar adsorption-desorption indicated the

Table 2
Comparative characteristics of silicate and aluminosilicate sorbents to Co^{2+} ions.

Sorbent	q, mg/g	Specific surface, m^2/g	Experiment conditions				
			Concentration of Co^{2+}	Solid/Liquid ratio	t, ºC	Time, h	pH
Kaolinite	11	3.8	10–250 mg/L	1:500	30	4	5.8
Montmorillonite[22]	28.6	19.8					
A mixture of natural zeolite phillipsite ($K_6(Si_{10}Al_6)O_{32}.12\,H_2O$) and bentonite[23]	2.73	–	5–50 mg/L	1:5		1–12	
Hydroxyl magnesium silicate $Mg_3Si_4O_{10}(OH)_2$[51]	3.85	–	20–50 mg/L	1:250	25–55	1–12	1–8
Natural	12.4	294–370	1–100 mg/L	1:500	25	2	8.5
Synthetic allophane ($1–2SiO_2{\cdot}Al_2O_3.5–6\,H_2O$)[21]	29.0						
Al-pillared bentonite clay[52]	38.6	227	10–400 mg/L		30–60	24	2.0–9.0
EDTA -modified silica gel[53]	20.0	–		1:500		4	3.0
Mesoporous Calcium Hydrosilicate[32]	154.8	733	25–500 mg/L	1:500	25–55	4	4.0–7.0
Amorphous Calcium Hydrosilicate $CaO{\cdot}SiO_2{\cdot}1.3\,H_2O$[46]	10	108.6	$0.34{\cdot}10^{-2}$ - 0.17 mmol/L	1:1000	20	3	2.0–10.0
Cancrinite-type zeolite from fly ash[54]	73.3	278.9	0.5 – 4 mmol/L	1:2000	25	72	6.0
Expanded perlite[55]	1.05	1.89	5 – 50 mg/L	1–18 g/L	20–50	5–360 min	2.0–8.0
Attapulgite (palygorskite)[56]	0.159	–	30–135 mg/L	1:250	10–40	16	
Bentonite	22	25		1:200	25–45	2	7.0
formaldehyde modified-bentonite[57]	34						
Modified montmorillonite (organically modified with thoron)[58]	46	–	0.4–7 mmol/L	1:100	30–60	1	4.2
Bentonite	7.924	–		1:25	30	1	5.8
montmorillonite	5.119			1:25		1	3.7
diatomite	8.721			1:25		1	3.7
sepiolite[59]	8.136			1:100		48	3.7
11 Å tobermorite from the remnants of the disposal of newsprint[26]	10.47	–	100 mg/L	1:20	20	1–120 min	1.0

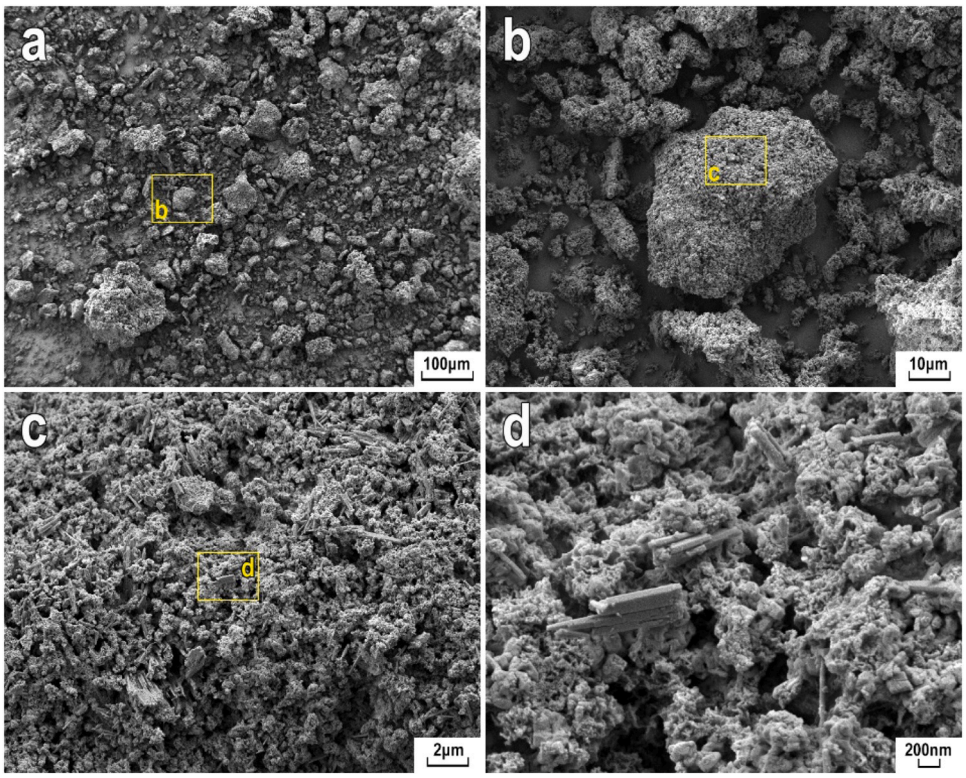

Fig. 4. SEM images of a sorbent saturated with Co^{2+} ions ($CaCoSi_2O_6$) at different magnification: a –× 0.5 K; b –× 2 K; c –× 10 K; d –× 50 K.

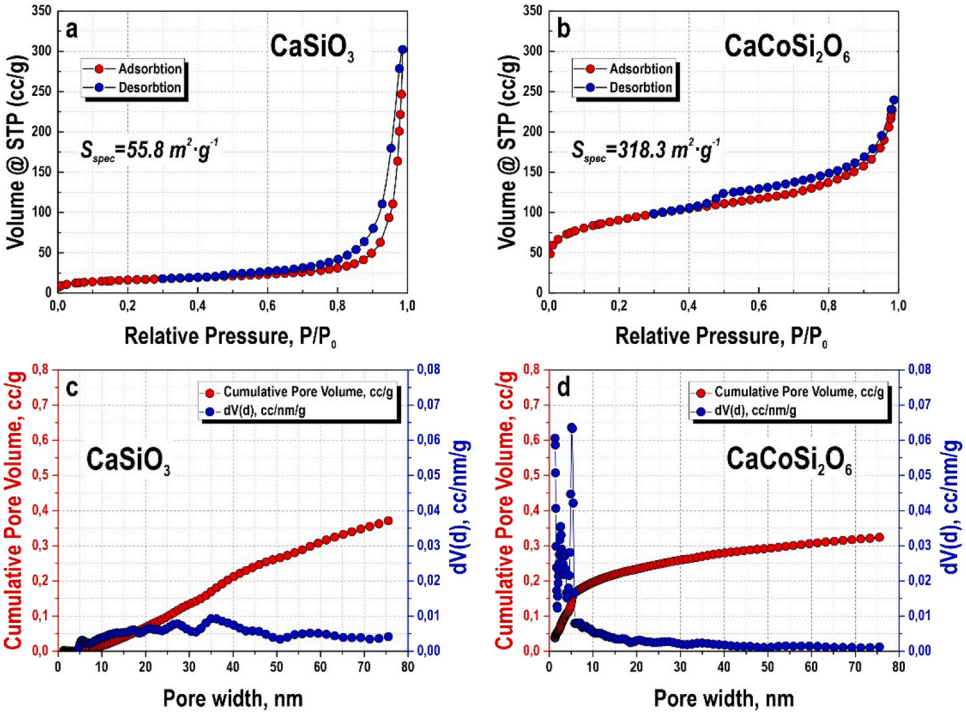

Fig. 5. (a, b) Isotherms of low-temperature N_2 adsorption-desorption and (c, d) DFT pore size distribution (a, c) of the initial ($CaSiO_3$) and (b, d) saturated with Co^{2+} ($CaCoSi_2O_6$) sorbents.

presence of a significant volume of micropores in the studied samples, which is confirmed by pronounced maxima on the pore size distribution curves in the region of 0.5–1.0 nm (Fig. 6c-f). The calculated values of the specific surface according to the Ar adsorption-desorption data were 43 and 300 m^2/g, which close to the data obtained from the N_2 adsorption-desorption.

According to the dilatometric curves of the shrinkage rate of the powder, it was determined that sintering proceeds in two stages (Fig. 7a). Stage I took place at the beginning of the process at the first minutes of synthesis (up to 2 min) and a temperature of up to 600 °C and was caused by the rearrangement and packing of particles under mechanical action during powder pressing. The shrinkage rate at

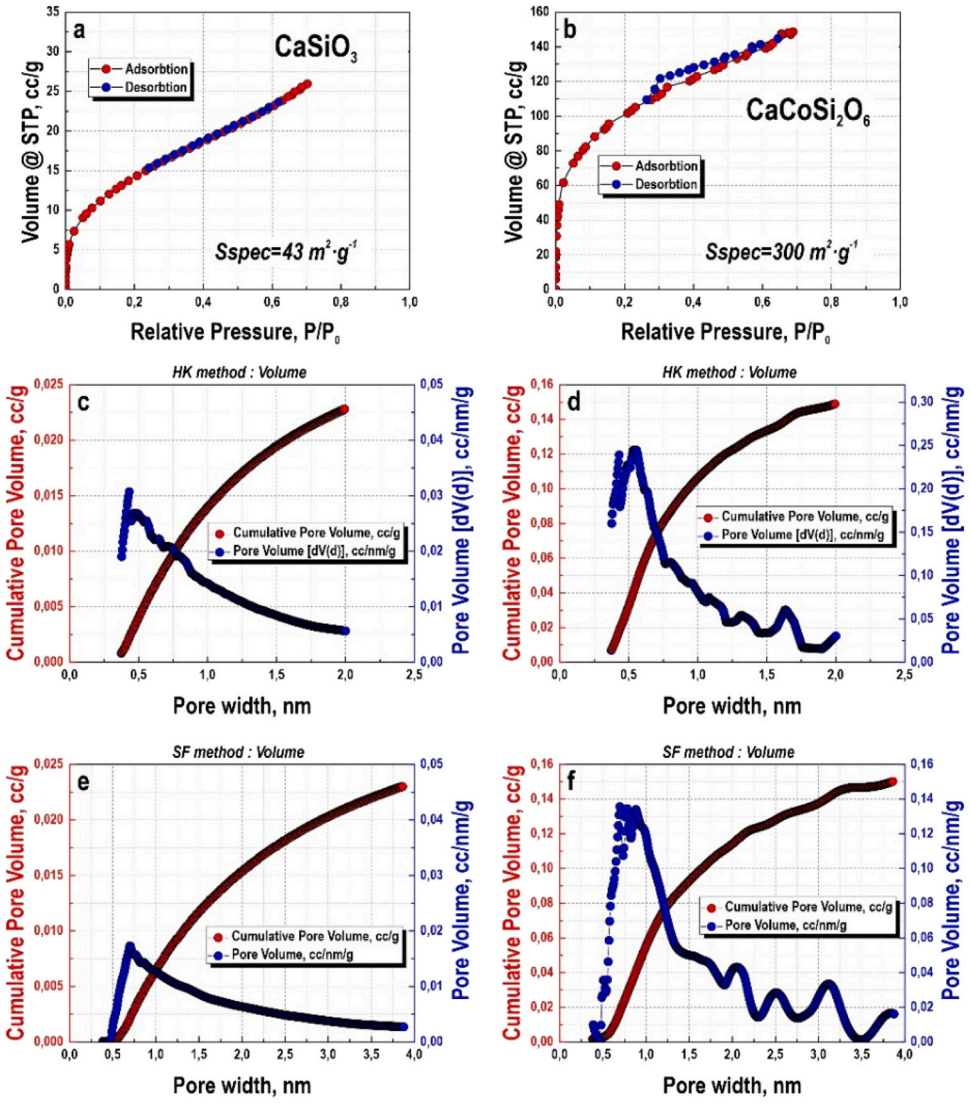

Fig. 6. (a, b) Isotherms of low-temperature Ar adsorption-desorption and (c-f) pore size distribution curves calculated by (c, d) HK and (e, f) SF (a, c, e) of the initial (CaSiO3) and (b, d, f) saturated with Co^{2+} ions ($CaCoSi_2O_6$) sorbents.

this stage was 6.5 mm/min, regardless of the sintering temperature. Stage II included thermal action on the powder along with the applied pressing pressure. This stage was intermediate and was primarily associated with the decomposition of calcium carbonate and the formation of calcium oxide, which was also involved in the sintering of the final product. Stage III was the main stage of sintering, since during heating, the processes of diffusion, plastic deformation and viscous flow of the material in the contact area of

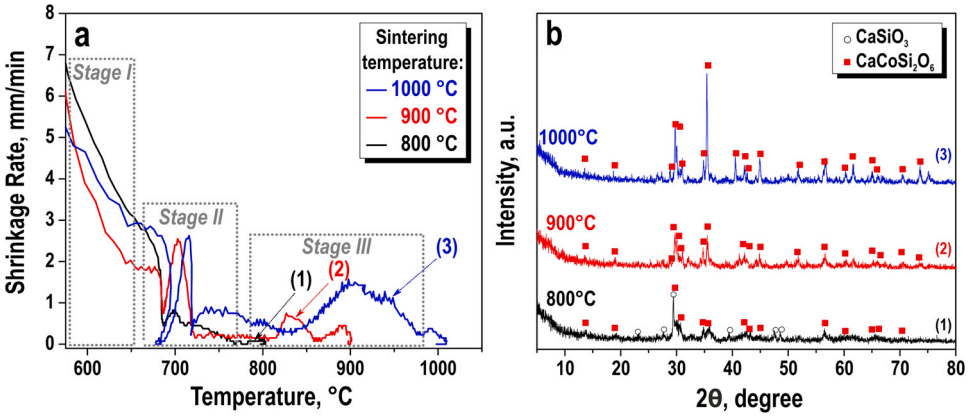

Fig. 7. (a) Shrinkage rates and (b) X-ray diffractograms of solid-state matrices obtained by SPS of a sorbent saturated with Co^{2+} ions ($CaCoSi_2O_6$) at various temperatures (800, 900, 1000 °C).

particles were activated, which intensified the shrinkage of the sintered powder. Thus, the sintering $CaCoSi_2O_6$ powder did not occur at a temperature of 800 °C, since there was no shrinkage at this stage (Fig. 7a). Intensive sintering was observed at 900 and 1000 °C, as supported by active shrinkage of the powder at a rate of 0.5 and 1.5 mm/min, respectively. The shrinkage time was no more than 2 min (Fig. 7a).

It is worth noting: the temperature from the pyrometer survey point (the outer or inner wall of the mold), aka the design temperature, and in the volume of the sample. Simulation data, using the consolidation of different systems as an example, are presented in papers [61–70]. In the mentioned works it was noted that the difference in temperature depends on the type of sintered material (conductor/semiconductor and dielectric). calculation of current distribution in the SPS process between the sample and the graphite head for single-phase conducting powders we, as well as the effect of self-joule heating of particles, shows the existence of a sharp temperature gradient from the particle interface to the particle center [67]. In the case of conductive materials and the minimum thickness of the mold wall in the area of contact with the material surface from which the temperature is determined, this difference is minimal, and for dielectrics does not exceed 50 °C. The temperature difference between the internal and external surfaces of the mold wall, which depends significantly on its thickness and can vary from 50° to 200°C, was investigated [71]. The temperature at the sampling point on the mold surface (design temperature) and the local actual temperature in the micro areas of the sample on the surface of the material grains are different. This is due to the mechanism of the SPS process (the mechanism of powder heating by pulse current). The main energy (Joule-Lentz heat) of sintering is generated at the grain boundary. At these points of contact, the material in the near-surface area can turn into a plasma state instantly. These are very small micro areas and their quantity in the entire sample volume can be quite large (but this does not mean that this effect is observed for each particle and in each contact). It is not possible to measure the temperature in such micro-areas. The total system temperature is measured after the heat from the micro areas is distributed and balanced throughout the sample.

According to the XRD data (Fig. 7a), the sample obtained at 800 °C includes crystalline $CaCoSi_2O_6$ with an admixture of the $CaSiO_3$. In the composition of the matrix obtained at 900 and 1000 °C, only the crystalline phase of calcium-cobalt silicate $CaCoSi_2O_6$ was identified, which indicates the complete interaction of the initial calcium silicate with sorbed Co^{2+} ions (Fig. 7b).

It should be noted that the entire cycle of thermal exposure to sintered mixtures did not exceed 10 min, which is an undeniable advantage of the SPS approach in terms of ensuring the safety of handling hazardous radionuclides. As a result of thermal consolidation, we have obtained a sample whose physico-mechanical properties were fairly considered to meet the requirements of handling and storage of this type of waste.

In order to visualize the crystal structures of silicate compounds obtained at 1000 °C (Fig. 8a), their structural 3D models were constructed (Fig. 8b) using VESTA software [18]. The parameters of the unit cell of calcium-cobalt silicate $CaCoSi_2O_6$ coincided with the calculated values and corresponded to the monoclinic form, where a= 9.806, b= 8.95, c= 5.243 Å. According to the obtained model, it can be seen how much cobalt is chemically bound in the silicate structure, due to which the $CaCoSi_2O_6$ matrix has extremely high stability, does not dissolve in water and organic solvents, while reacting with hydrochloric acid.

The structure of sintered samples varied depending on the calcination temperature (Fig. 9). The SEM image of the surface of the longitudinal cleavage of the sample obtained at 800 °C shows that sintering processes were only initiated. The sample volume contained both sintered areas in the form of monolithic inclusions, and

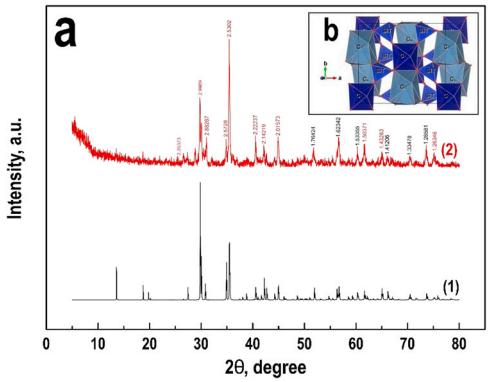

Fig. 8. (a) X-ray diffractogame (2) of the $CaCoSi_2O_6$ sample obtained at 1000 °C, (1) of the reference structure, and (b) a model image of the $CaCoSi_2O_6$ crystal structure.

loose ones in the form of compressed and partially sintered particles of the initial powder (Fig. 9a, a*). The sample surface had a high porosity, due to the decomposition of calcium carbonate with the formation of carbon dioxide, which was a pore-forming agent. When the temperature increased to 900 °C, the density of monolithic agglomerates increased significantly due to the intensification of sintering processes, however, the presence of an insignificant number of microdefects in the sample volume was detected (Fig. 9b, b*). When the temperature reached 1000 °C, the matrix sample had a monolithic, nonporous and defect-free structure (Fig. 9c, c *).

According to the EDX analysis data (Fig. 9), the distribution of the cobalt and silicon elements over the surface of the matrix samples should be considered uniform and differ to calcium. Meanwhile, the cobalt was integrated throughout the entire volume of the matrices. It is established that the physical and mechanical characteristics of $CaCoSi_2O_6$ samples were in direct proportion to the SPS temperature. Density, compressive strength and Vickers microhardness increased with increasing sintering temperature (Table 3). These parameters increased sharply at sintering temperatures from 900 °C and above, which indicates the efficiency of $CaCoSi_2O_6$ powder sintering under these conditions and was consistent with the previously noted powder shrinkage kinetics (Fig. 7a).

The metal ions leaching from the obtained $CaCoSi_2O_6$ matrices was evaluated, which is the main indicator of their effectiveness for the immobilization of cobalt radionuclides (Table 4, Fig. 10). The lowest Co^{2+} leaching rate was observed for samples obtained at 800 and 900 °C (Table 4). This parameter was $(2.55–2.39)\times 10^{-7}$ g/cm^2·day, which meets the requirements of GOST R 50926–96 for solidified high-level waste. Similar results were obtained for the parameters of the leaching depth and the leaching index (Table 4).

Obviously, the low metal ions leaching from silicate matrices was due to their glass-like composition. The increase in this indicator for samples obtained at an elevated sintering temperature was due to the formation of the calcium-cobalt silicate confirmed by XRD (Fig. 8a) and the formation of a monolithic structure (Fig. 9c, c*).

According to the de Groot and der Slot model [43], the tangent of the angle of inclination of the tangent to the line of dependence of the logarithm of the leached fraction of the component on the logarithm of time is associated with the mechanism of leaching from the matrices. A value of 0.5 indicates a purely diffusive removal of the substance, 1 - the dissolution of the surface of the samples, and 0 - the effect of surface flushing. The tangent of the angle of inclination of a straight line at 800 °C was 0.6692, when for samples prepared at 900 and 1000 °C were 0.7387 (Fig. 11a). Thus, it indicated about the complex Co^{2+} leaching mechanism. For the sample obtained at 800 °C was due to a greater extent to the processes of diffusion removal from the matrices volume. Samples obtained at higher temperatures were characterized by a relatively large contribution of the

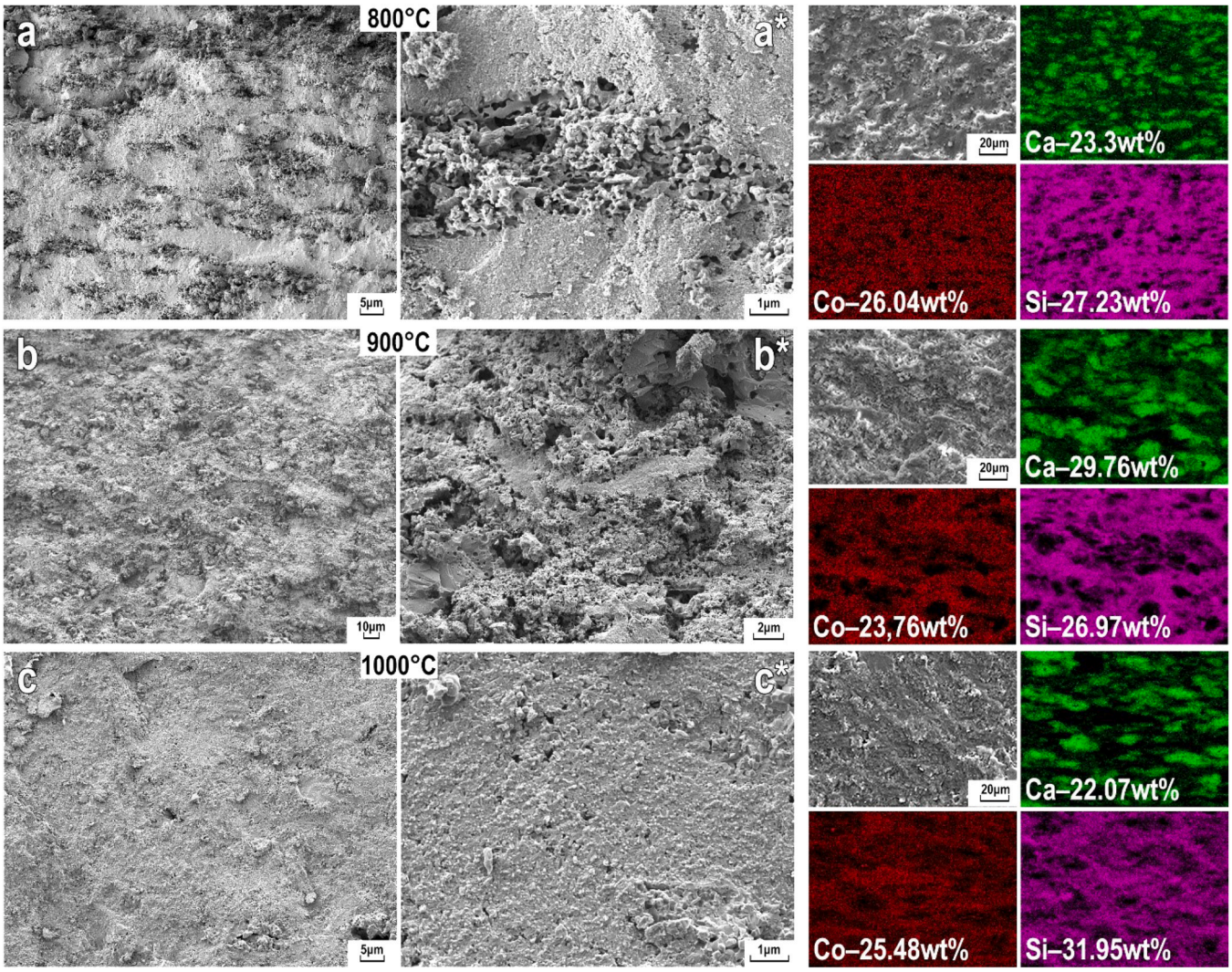

Fig. 9. SEM images and EDX mapping of $CaCoSi_2O_6$ matrices obtained at different SPS temperatures (800, 900, 1000 °C).

Table 3
Physico-mechanical properties of $CaCoSi_2O_6$ matrices obtained at different SPS temperatures (800, 900, 1000 °C).

Temperature, °C	Density, g/cm^3	Compressive strength, MPa	Hardness, GPa
800	2.81	150	1.80
900	3.05	212	4.80
1000	3.16	637	5.25

dissolution processes of the carrier matrices, comparable to diffusion removal. The dense structure of the samples obtained at high temperatures reduced the mobility of Co^{2+} ions, while accelerating the dissolution of the sample.

The leaching depths were calculated as a function of time (Fig. 11b), which can be used as a characteristic of the solubility of the matrices. It was shown that the obtained matrices were stable in distilled water. The sample obtained at 800 °C was characterized by the highest leaching depth, which is consistent with the previously established contribution of the predominantly diffusion mechanism of Co^{2+} ions from the sample, and it was explained by a comparison of silicate samples densities. The density of the sample obtained at 1000 °C was 1.3 times greater than that of the matrices obtained at 800 °C (Table 3). Thus, with comparable diffusion coefficients, the amount of dissolved Co^{2+} ions of a high-temperature sample were significantly higher, which ensures a diffusion and dissolution leaching mechanism contribution. The leaching index (L) of all samples was significantly higher than 8, which allowed us to conclude that Co^{2+} ions are reliably immobilized in the volume of the material and the prepared matrices can be used to ^{60}Co radionuclides immobilization [3].

Table 4
Parameter of Co^{2+} ions leaching after 30 days.

Temperature, °C	Diffusion coefficient, cm^2/s	Leaching rate Co^{2+}, g/ (cm^2 ×day)	Leaching index	Leaching depth, cm
800	2.70×10^{-17}	3.04×10^{-7}	16.59	4.72×10^{-6}
900	1.78×10^{-17}	2.39×10^{-7}	16.57	4.23×10^{-6}
1000	1.73×10^{-17}	2.25×10^{-7}	16.76	3.50×10^{-6}

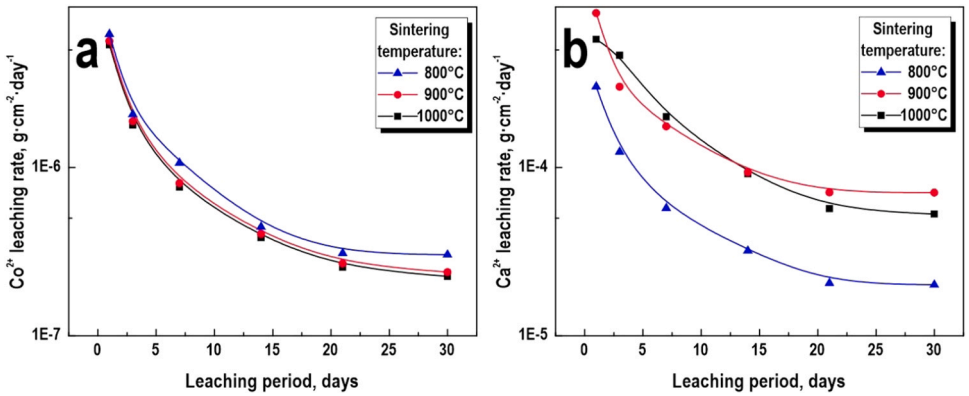

Fig. 10. (a) leaching rate of Co^{2+} and (b) Ca^{2+} ions from $CaCoSi_2O_6$ matrices obtained at different SPS temperatures (800, 900, 1000 °C).

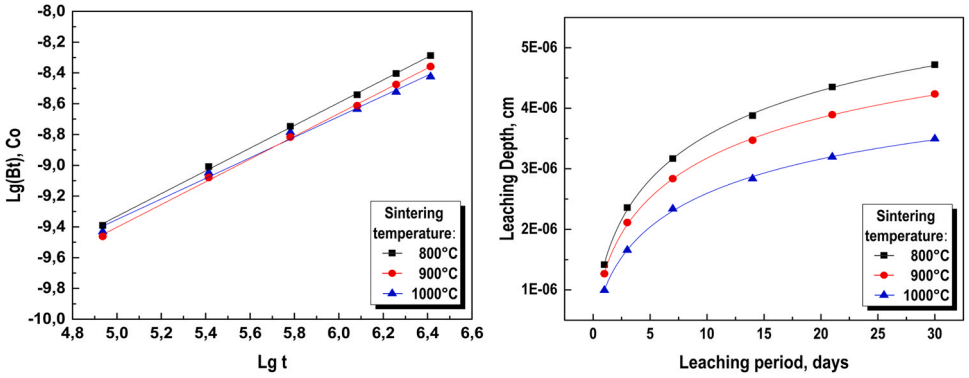

Fig. 11. The plots of (a) lg(Bt) vs lgt and (b) the leaching depth *vs* t for $CaCoSi_2O_6$ matrices obtained at different SPS temperatures (800, 900, 1000 °C).

4. Conclusions

Amorphous $CaSiO_3$ silicate with a high sorption capacity to Co^{2+} ions 3.32 mmol/g was synthesized by precipitation from an alkaline solution of sodium metasilicate and calcium chloride. Solid-state matrices of crystalline composition based on $CaCoSi_2O_6$ were obtained by SPS at 800–1000 °C. The thermal stability of the initial ($CaSiO_3$) and saturated with Co^{2+} ions ($CaCoSi_2O_6$) samples during heat treatment in an inert medium up to 1200 °C was shown. The obtained by SPS $CaCoSi_2O_6$ matrices with a uniform distribution of cobalt by volume had high values of density (3.16 g/cm^3), compressive strength (150–637 MPa) and Vickers microhardness (1.80–5.25 GPa). The sample obtained at 1000 °C had the lowest metal ions leaching, for which the cobalt leaching rate (R_{Co}) did not exceed 10^{-7} g/cm·day, the diffusion coefficient (De) was 1.73×10^{-17} cm^2/s. The high efficacy of the obtained silicate matrices was confirmed by compliance with GOST R 50926–96, ANSI/ANS 16.1. The prepared $CaCoSi_2O_6$ silicate matrices are of practical interest for technologies of purification and processing of radioactive waste.

CRediT authorship contribution statement

Shichalin O.O.: Writing - review & editing, results discussion. **Yarusova S.B.:** Conceptualization, Methodology, Writing – original draft. **Andrei Ivanets:** Formal analysis & Results discussion, Editing. **Papynov E.K.:** Project administration, Funding acquisition, Editing. **Belov A.A.:** Ceramic matrix, sintering. **Azon S.A.:** Adsorption experiments, g(Bt) vs lgt and the leaching depth. **Buravlev I.Yu.:** Visualization, Data curation. **Zadorozhny P.A.:** Cobalt analysis by AAC, pH solution analysis. **Panasenko A.E.:** Visualization, Data curation. **Mayorov V.Yu.:** N2 and Ar adsorption-desorption measurements. **Shlyk D. Kh.:** XRD analysis. **Nepomnyushchaya V.A.:** Investigation, Formal analysis. **Kapustina O.V.:** Investigation, Validation. **Ivanova A.E.:** Investigation. **Buravleva A.A.:** Data curation, Formal analysis. **Merkulov E.B.:** DTA/TG analysis. **Gordienko P.S.:** Conceptualization, Data curation, Formal analysis.

Declaration of Competing Interest

The authors declare that they have no known competing financial interests or personal relationships that could have appeared to influence the work reported in this paper.

Acknowledgments

The synthesis and characterization of the ceramics samples were funded by the State Assignment of the Ministry of Science and Higher Education of the Russian Federation No. 00657–2020-0006. Sorbent synthesis, its characterization, saturation with Co ions, XRD and AAS (determination of Ca^{2+}, Co^{2+} concentration) analysis were funded by the State Order of the Institute of Chemistry FEB RAS topic number 0205–2021-0002. The work involved equipment of integrated common use center and interdisciplinary in the field of nanotechnologies and new functional materials (Far Eastern Federal University, Vladivostok, Russia), and metal concentration were determined using equipment of the Far East Center of Structural Studies (Institute of Chemistry, Far Eastern Branch of the Russian Academy of Sciences, Vladivostok, Russia).

References

[1] S.M. Yu, A.P. Ren, C.L. Chen, Y.X. Chen, X. Wang, Effect of pH, ionic strength and fulvic acid on the sorption and desorption of cobalt to bentonite, Appl. Radiat. Isot. 64 (2006) 455–461, https://doi.org/10.1016/j.apradiso.2005.08.019

[2] F. Qureshi, S.Q. Memon, M.Y. Khuhawar, T.M. Jahangir, A.H.H. Channar, Synthesis and application of fluorescent and thermally stable polyazomethine as

adsorbent in the remediation of Ni (II), Cu (II) and Co (II) from wastewater systems, J. Polym. Res. 28 (2021), https://doi.org/10.1007/s10965-021-02582-2
[3] F. Qureshi, S.Q. Memon, M.Y. Khuhawar, T.M. Jahangir, Removal of Co2+, Cu2+ and Au3+ ions from contaminated wastewater by using new fluorescent and antibacterial polymer as sorbent, Polym. Bull. 78 (2021) 1505–1533, https://doi.org/10.1007/s00289-020-03170-y
[4] N. Samadi, R. Hasanzadeh, M. Rasad, Adsorption isotherms, kinetic, and desorption studies on removal of toxic metal ions from aqueous solutions by polymeric adsorbent, J. Appl. Polym. Sci. 132 (2015) 1–13, https://doi.org/10.1002/app.41642
[5] H. Al-Shahrani, F. Alakhras, E. Al-Abbad, G. Al-Mazaideh, A. Hosseini-Bandegharaei, N. Ouerfelli, Sorption of cobalt (II) ions from aqueous solutions using chemically modified chitosan, Glob. Nest J. 20 (2018) 620–627, https://doi.org/10.30955/gnj.002804
[6] A.I. Ivanets, V. Srivastava, N.V. Kitikova, I.L. Shashkova, M. Sillanpää, Kinetic and thermodynamic studies of the Co(II) and Ni(II) ions removal from aqueous solutions by Ca-Mg phosphates, Chemosphere 171 (2017) 348–354, https://doi.org/10.1016/j.chemosphere.2016.12.062
[7] M. Maslova, N. Mudruk, A. Ivanets, I. Shashkova, N. Kitikova, A novel sorbent based on Ti-Ca-Mg phosphates: synthesis, characterization, and sorption properties, Environ. Sci. Pollut. Res. 27 (2020) 3933–3949, https://doi.org/10.1007/s11356-019-06949-3
[8] C. Das, S. Sen, T. Singh, T. Ghosh, S.S. Paul, T.W. Kim, S. Jeon, D.K. Maiti, J. Im, G. Biswas, Green synthesis, characterization and application of natural product coated magnetite nanoparticles for wastewater treatment, Nanomaterials 10 (2020) 1–19, https://doi.org/10.3390/nano10081615
[9] S. Tizro, H. Baseri, Removal of cobalt ions from contaminated water using magnetite based nanocomposites: effects of various parameters on the removal efficiency, J. Water Environ. Nanotechnol. J. Water Environ. Nanotechnol. 2 (2017) 174–185 doi:10.22090/..
[10] M. Mohapatra, L. Mohapatra, P. Singh, S. Anand, B. Mishra, A comparative study on Pb(II), Cd(II), Cu(II), Co(II) adsorption from single and binary aqueous solutions on additive assisted nano-structured goethite, Int. J. Eng. Sci. Technol. 2 (2011) 89–103, https://doi.org/10.4314/ijest.v2i8.63784
[11] E.J. Boyle-Wight, L.E. Katz, K.F. Hayes, Spectroscopic studies of the effects of selenate and selenite on cobalt sorption to γ-Al 2 O 3, Environ. Sci. Technol. 36 (2002) 1219–1225, https://doi.org/10.1021/es001774i
[12] S.B. Yarusova, N.V. Makarenko, P.S. Gordienko, M.A. Karpenko, E.S. Novikova, Effect of temperature on the kinetics of sorption of Co2+ and Ni2+ ions by a sorbent based on an inositol hexaphosphoric acid derivative, Russ. J. Phys. Chem. A. 92 (2018) 559–564, https://doi.org/10.1134/S0036024418030354
[13] H. Mohapatra, R. Gupta, Concurrent sorption of Zn(II), Cu(II) and Co(II) by Oscillatoria angustissima as a function of pH in binary and ternary metal solutions, Bioresour. Technol. 96 (2005) 1387–1398, https://doi.org/10.1016/j.biortech.2004.11.004
[14] J. Marešová, M. Pipíška, M. Rozložník, M. Horník, L. Remenárová, J. Augustín, Cobalt and strontium sorption by moss biosorbent: Modeling of single and binary metal systems, Desalination 266 (2011) 134–141, https://doi.org/10.1016/j.desal.2010.08.014
[15] S.V. Yudintsev, S.V. Stefanovsky, M.Y. Kalenova, B.S. Nikonov, M.S. Nikol'Skii, A.M. Koshcheev, A.S. Shchepin, Matrices for immobilization of the rare earth-actinide waste fraction, synthesized by cold crucible induction melting, Radiochemistry 57 (2015) 321–333, https://doi.org/10.1134/S1066362215030133
[16] N.P. Laverov, S.V. Yudintsev, S.V. Stefanovskii, B.I. Omel'Yanenko, B.S. Nikonov, Murataite matrices for actinide wastes, Radiochemistry 53 (2011) 229–243, https://doi.org/10.1134/S1066362211030027
[17] V.N. Mineev, A.S. Vlasov, A.P. Parshin, S.A. Mel'nikov, A.S. Shul'gin, Y.A. Zeigarnik, G.E. Val'yano, F.A. Akopov, O.M. Traktuev, S.V. Stefanovskii, Formation of mineral-like matrices for immobilization of fuel and fission products during a serious accident in a nuclear reactor, . Energy 95 (2003) 852–855, https://doi.org/10.1023/B:ATEN.0000018998.51535.17
[18] A.I. Orlova, M.I. Ojovan, Ceramic mineral waste-forms for nuclear waste immobilization, Mater. (Basel) 12 (2019), https://doi.org/10.3390/ma12162638
[19] C.C. Lin, A review of corrosion product transport and radiation field buildup in boiling water reactors, Prog. Nucl. Energy 51 (2009) 207–224, https://doi.org/10.1016/j.pnucene.2008.05.005
[20] S.A. Khan, Sorpt. Long. -lived Radionucl. cesium-134, strontium-85 Cobalt-60 bentonite 258 (2003) 3–6.
[21] A. Baldermann, A. Grießbacher, C. Baldermann, B. Purgstaller, I. Letofsky-Papst, S. Kaufhold, M. Dietzel, Removal of Barium, Cobalt, Strontium, and Zinc from Solution by Natural and Synthetic Allophane Adsorbents, Geosciences 8 (2018) 309, https://doi.org/10.3390/geosciences8090309
[22] K.G. Bhattacharyya, S. Sen Gupta, Kaolinite and montmorillonite as adsorbents for Fe(III), Co(II) and Ni(II) in aqueous medium, Appl. Clay Sci. 41 (2008) 1–9, https://doi.org/10.1016/j.clay.2007.09.005
[23] R.A.A. Dwairi, A.E. Al-Rawajfeh, Removal of cobalt and nickel from wastewater by using jordan low-cost zeolite and bentonite, J. Univ. Chem. Technol. Metall. 47 (2012) 69–76.
[24] A. Baldermann, V. Preissegger, S. Šimić, I. Letofsky-Papst, F. Mittermayr, M. Dietzel, Uptake of aqueous heavy metal ions (Co2+, Cu2+ and Zn2+) by calcium-aluminium-silicate-hydrate gels, Cem. Concr. Res 147 (2021), https://doi.org/10.1016/j.cemconres.2021.106521
[25] A. Baldermann, A. Landler, F. Mittermayr, I. Letofsky-Papst, F. Steindl, I. Galan, M. Dietzel, Removal of heavy metals (Co, Cr, and Zn) during calcium–aluminium–silicate–hydrate and trioctahedral smectite formation, J. Mater. Sci. 54 (2019) 9331–9351, https://doi.org/10.1007/s10853-019-03541-5
[26] N.J. Coleman, D.S. Brassington, A. Raza, A.P. Mendham, Sorption of Co2+ and Sr2+ by waste-derived 11 Å tobermorite, Waste Manag 26 (2006) 260–267, https://doi.org/10.1016/j.wasman.2005.01.019
[27] L.V. Akat'eva, V.K. Ivanov, S.A. Kozyukhin, V.D. Gladun, A.E. Baranchikov, V.I. Zhilov, A.I. Khol'kin, Using extraction and sorption processes to obtain nanosized powders of calcium silicates and functional materials on their basis, Theor. Found. Chem. Eng. 50 (2016) 490–497, https://doi.org/10.1134/S0040579516040023
[28] L.V. Akat'eva, A.E. Baranchikov, V.K. Ivanov, A.I. Khol'kin, Preparation of calcium silicates with long-fiber (needle) particles, Theor. Found. Chem. Eng. 49 (2015) 736–742, https://doi.org/10.1134/S0040579515050036
[29] P.S. Gordienko, S.B. Yarusova, S.B. Bulanova, V.A. Kolzunov, A.P. Suponina, K.N. Galkin, Calcium monosilicates as components of composite materials, Theor. Found. Chem. Eng. 44 (2010) 461–466, https://doi.org/10.1134/S0040579510040160
[30] S.B. Yarusova, P.S. Gordienko, A.A. Yudakov, Y.A. Azarova, R.D. Yashchuk, Kinetics of the sorption of heavy-metal ions by a sorbent obtained from boric acid production waste, Theor. Found. Chem. Eng. 50 (2016) 841–845, https://doi.org/10.1134/S0040579516050250
[31] E.I. Al-Wakeel, S.A. El-Korashy, S.A. El-Hemaly, M.A. Rizk, Divalent ion uptake of heavy metal cations by (aluminum + alkali metals) - Substituted synthetic 1.1 nm-tobermorites, J. Mater. Sci. 36 (2001) 2405–2415, https://doi.org/10.1023/A:1017969729433
[32] G. Qi, X. Lei, L. Li, C. Yuan, Y. Sun, J. Chen, J. Chen, Y. Wang, J. Hao, Preparation and evaluation of a mesoporous calcium-silicate material (MCSM) from coal fly ash for removal of Co(II) from wastewater, Chem. Eng. J. 279 (2015) 777–787, https://doi.org/10.1016/j.cej.2015.05.077
[33] O.O. Shichalin, E.K. Papynov, V.Y. Maiorov, A.A. Belov, E.B. Modin, I.Y. Buravlev, Y.A. Azarova, A.V. Golub, E.A. Gridasova, A.E. Sukhorada, I.G. Tananaev, V.A. Avramenko, Spark Plasma Sintering of Aluminosilicate Ceramic Matrices for Immobilization of Cesium Radionuclides, Radiochemistry 61 (2019) 185–191, https://doi.org/10.1134/S1066362219020097
[34] E.K. Papynov, O.O. Shichalin, A.Y. Mironenko, A.V. Ryakov, I.V. Manakov, P.V. Makhrov, I.Y. Buravlev, I.G. Tananaev, V.A. Avramenko, V.I. Sergienko, Synthesis of high-density pellets of uranium dioxide by spark plasma sintering in dies of different types, Radiochemistry 60 (2018) 362–370, https://doi.org/10.1134/S1066362218040045
[35] O.O. Shichalin, E.K. Papynov, V.A. Nepomnyushchaya, A.I. Ivanets, A.A. Belov, A.N. Dran'kov, S.B. Yarusova, I.Y. Buravlev, A.E. Tarabanova, A.N. Fedorets, S.A. Azon, Z.E. Kornakova, S.Y. Budnitskiy, I.G. Tananaev, Y. Shi, Y. Xiong, H. Wang, Hydrothermal synthesis and spark plasma sintering of NaY zeolite as solid-state matrices for cesium-137 immobilization, J. Eur. Ceram. Soc. (2022), https://doi.org/10.1016/j.jeurceramsoc.2022.02.007
[36] E.K. Papynov, O.O. Shichalin, M.A. Medkov, D.N. Grishchenko, I.A. Tkachenko, A.N. Fedorets, V.S. Pechnikov, A.V. Golub, I.Y. Buravlev, I.G. Tananaev, V.A. Avramenko, Spark plasma sintering of special-purpose functional ceramics based on UO2, ZrO2, Fe3O4/α-Fe2O3, Glas. Phys. Chem. 44 (2018) 632–640, https://doi.org/10.1134/S1087659618060159
[37] E.K. Papynov, O.O. Shichalin, V.Y. Mayorov, V.G. Kuryavyi, T.A. Kaidalova, SPS technique for ionizing radiation source fabrication based on dense cesium-containing core, J. Hazard. Mater. 369 (2019) 25–30, https://doi.org/10.1016/j.jhazmat.2019.02.016
[38] E.K. Papynov, O.O. Shichalin, A.A. Belov, I.Y. Buravlev, A.S. Portnyagin, S.A. Azon, D.K. Shlyk, A.A. Buravleva, Y.A. Parot'kina, V.A. Nepomnyushchaya, Z.E. Kornakova, A.V. Gridasov, I.G. Tananaev, V.I. Sergienko, Synthesis of Mineral-Like SrWO4 Ceramics with the Scheelite Structure and a Radioisotope Product Based on It, Russ. J. Inorg. Chem. 66 (2021) 1434–1446, https://doi.org/10.1134/S0036023621090114
[39] E.K. Papynov, A.A. Belov, O.O. Shichalin, I.Y. Buravlev, S.A. Azon, A.V. Golub, A.V. Gerasimenko, Y.A Parotkina, A.P. Zavjalov, I.G. Tananaev, V.I. Sergienko, SrAl2Si2O8 ceramic matrices for 90Sr immobilization obtained via spark plasma sintering-reactive synthesis, Nucl. Eng. Technol. (2021) 2–7, https://doi.org/10.1016/j.net.2021.01.024
[40] E.K. Papynov, O.O. Shichalin, I.Y. Buravlev, A.S. Portnyagin, A.A. Belov, V.Y. Maiorov, Y.E. Skurikhina, E.B. Merkulov, V.O. Glavinskaya, A.D. Nomerovskii, A.V. Golub, N.P. Shapkin, Reactive spark plasma synthesis of porous bioceramic wollastonite, Russ. J. Inorg. Chem. 65 (2020) 263–270, https://doi.org/10.1134/S0036023620020138
[41] E.K. Papynov, O.O. Shichalin, I.Y. Buravlev, A.A. Belov, A.S. Portnyagin, A.N. Fedorets, Y.A. Azarova, I.G. Tananaev, V.I. Sergienko, Spark plasma sintering-reactive synthesis of SrWO4 ceramic matrices for 90Sr immobilization, Vacuum 180 (2020) 109628, https://doi.org/10.1016/j.vacuum.2020.109628
[42] S.B. Yarusova, O.O. Shichalin, A.A. Belov, S.A. Azon, I.Y. Buravlev, A.V. Golub, V.Y. Mayorov, A.V. Gerasimenko, E.K. Papynov, A.I. Ivanets, A.A. Buravleva, E.B. Merkulov, V.A. Nepomnyushchaya, O.V. Kapustina, P.S. Gordienko, Synthesis of amorphous KAlSi3O8 for cesium radionuclide immobilization into solid matrices using spark plasma sintering technique, Ceram. Int. (2021), https://doi.org/10.1016/j.ceramint.2021.10.164
[43] L.H.H.A. van der Sleet, Ph. Quevauviller, Harmonization of Leaching/ Extraction Tests, 1998.
[44] D. Daval, I. Martinez, J. Corvisier, N. Findling, B. Goffé, F. Guyot, Carbonation of Ca-bearing silicates, the case of wollastonite: Experimental investigations and kinetic modeling, Chem. Geol. 265 (2009) 63–78, https://doi.org/10.1016/j.chemgeo.2009.01.022
[45] F. Di Lorenzo, C. Ruiz-Agudo, A. Ibañez-Velasco, R. Gil-San Millán, J.A.R. Navarro, E. Ruiz-Agudo, C. Rodriguez-Navarro, The carbonation of wollastonite: A model

reaction to test natural and biomimetic catalysts for enhanced CO_2 sequestration, Minerals 8 (2018), https://doi.org/10.3390/min8050209
[46] P.S. Gordienko, S.B. Yarusova, A.P. Suponina, A.A. Yudakov, I.G. Zhevtun, Effect of hydration and air exposure on sorption properties and phase composition of calcium silicate hydrate, Russ. J. Gen. Chem. 84 (2014) 2596–2602, https://doi.org/10.1134/S1070363214130179
[47] M. Shokrollahi Yancheshmeh, H.R. Radfarnia, M.C. Iliuta, High temperature CO_2 sorbents and their application for hydrogen production by sorption enhanced steam reforming process, Chem. Eng. J. 283 (2016) 420–444, https://doi.org/10.1016/j.cej.2015.06.060
[48] X. Yan, Y. Li, X. Ma, J. Zhao, Z. Wang, Performance of Li4SiO4 material for CO_2 capture: A review, Int. J. Mol. Sci. 20 (2019), https://doi.org/10.3390/ijms20040928
[49] Y. Hu, W. Liu, Y. Yang, M. Qu, H. Li, CO_2 capture by Li4SiO4 sorbents and their applications: Current developments and new trends, Chem. Eng. J. 359 (2019) 604–625, https://doi.org/10.1016/j.cej.2018.11.128
[50] A.I. Rat'Ko, A.I. Ivanets, A.I. Kulak, E.A. Morozov, I.O. Sakhar, Thermal decomposition of natural dolomite, Inorg. Mater. 47 (2011) 1372–1377, https://doi.org/10.1134/S0020168511120156
[51] M.M. Hamed, M. Holiel, I.M. Ahmed, Sorption behavior of cesium, cobalt and europium radionuclides onto hydroxyl magnesium silicate, Radiochim. Acta 104 (2016) 873–890, https://doi.org/10.1515/ract-2016-2579
[52] D.M. Manohar, B.F. Noeline, T.S. Anirudhan, Adsorption performance of Al-pillared bentonite clay for the removal of cobalt(II) from aqueous phase, Appl. Clay Sci. 31 (2006) 194–206, https://doi.org/10.1016/j.clay.2005.08.008
[53] E. Repo, T.A. Kurniawan, J.K. Warchol, M.E.T. Sillanpää, Removal of Co(II) and Ni (II) ions from contaminated water using silica gel functionalized with EDTA and/or DTPA as chelating agents, J. Hazard. Mater. 171 (2009) 1071–1080, https://doi.org/10.1016/j.jhazmat.2009.06.111
[54] W. Qiu, Y. Zheng, Removal of lead, copper, nickel, cobalt, and zinc from water by a cancrinite-type zeolite synthesized from fly ash, Chem. Eng. J. 145 (2009) 483–488, https://doi.org/10.1016/j.cej.2008.05.001
[55] H. Ghassabzadeh, M. Torab-Mostaedi, A. Mohaddespour, M.G. Maragheh, S.J. Ahmadi, P. Zaheri, Characterizations of Co (II) and Pb (II) removal process from aqueous solutions using expanded perlite, Desalination 261 (2010) 73–79, https://doi.org/10.1016/j.desal.2010.05.028
[56] H. Chiu, J. Wang, Adsorpt. Thermodyn. Cobalt Ions onto Attapulgite 3 (2009) 102–106.
[57] H. Omar, H. Arida, A. Daifullah, Adsorption of 60Co radionuclides from aqueous solution by raw and modified bentonite, Appl. Clay Sci. 44 (2009) 21–26, https://doi.org/10.1016/j.clay.2008.12.013
[58] M.A. Soliman, G.M. Rashad, M.R. Mahmoud, Organo-modification of montmorillonite for enhancing the adsorption efficiency of cobalt radionuclides from aqueous solutions, Environ. Sci. Pollut. Res. 26 (2019) 10398–10413, https://doi.org/10.1007/s11356-019-04478-7
[59] G.M. Rashad, M.R. Mahmoud, A.M. Elewa, E. Metwally, E.A. Saad, Removal of radiocobalt from aqueous solutions by adsorption onto low-cost adsorbents, J. Radioanal. Nucl. Chem. 309 (2016) 1065–1076, https://doi.org/10.1007/s10967-016-4726-4
[60] M. Thommes, K. Kaneko, A.V. Neimark, J.P. Olivier, F. Rodriguez-Reinoso, J. Rouquerol, K.S.W. Sing, Physisorption of gases, with special reference to the evaluation of surface area and pore size distribution (IUPAC Technical Report), Pure Appl. Chem. 87 (2015) 1051–1069, https://doi.org/10.1515/pac-2014-1117
[61] C. Manière, L. Durand, E. Brisson, H. Desplats, P. Carré, P. Rogeon, C. Estournès, Contact resistances in spark plasma sintering: From in-situ and ex-situ determinations to an extended model for the scale up of the process, J. Eur. Ceram. Soc. 37 (2017) 1593–1605, https://doi.org/10.1016/j.jeurceramsoc.2016.12.010
[62] X. Liu, X. Song, S. Zhao, J. Zhang, Spark plasma sintering densification mechanism for cemented carbides with different WC particle sizes, J. Am. Ceram. Soc. 93 (2010) 3153–3158, https://doi.org/10.1111/j.1551-2916.2010.03862.x
[63] C. Manière, E. Torresani, E. Olevsky, Simultaneous spark plasma sintering of multiple complex shapes, Mater. (Basel) 12 (2019) 557, https://doi.org/10.3390/ma12040557
[64] C. Manière, G. Lee, E.A. Olevsky, All-materials-inclusive flash spark plasma sintering, Sci. Rep. 7 (2017) 15071, https://doi.org/10.1038/s41598-017-15365-x
[65] E. Govea-Alcaide, J.E. Pérez-Fernández, I.F. Machado, R.F. Jardim, The spatial distribution of temperature and oxygen deficiency in spark-plasma sintered superconducting Bi-based materials, Phys. B Condens. Matter 455 (2014) 35–38, https://doi.org/10.1016/j.physb.2014.07.040
[66] M. Sakkaki, F. Sadegh Moghanlou, M. Vajdi, M. Shahedi Asl, M. Mohammadi, M. Shokouhimehr, Numerical simulation of heat transfer during spark plasma sintering of zirconium diboride, Ceram. Int. 46 (2020) 4998–5007, https://doi.org/10.1016/j.ceramint.2019.10.240
[67] X. Song, X. Liu, J. Zhang, Neck formation and self-adjusting mechanism of neck growth of conducting powders in spark plasma sintering, J. Am. Ceram. Soc. 89 (2006) 494–500, https://doi.org/10.1111/j.1551-2916.2005.00777.x
[68] G. Lee, E.A. Olevsky, C. Manière, A. Maximenko, O. Izhvanov, C. Back, J. McKittrick, Effect of electric current on densification behavior of conductive ceramic powders consolidated by spark plasma sintering, Acta Mater. 144 (2018) 524–533, https://doi.org/10.1016/j.actamat.2017.11.010
[69] G. Antou, G. Mathieu, G. Trolliard, A. Maître, Spark plasma sintering of zirconium carbide and oxycarbide: Finite element modeling of current density, temperature, and stress distributions, J. Mater. Res. 24 (2009) 404–412, https://doi.org/10.1557/JMR.2009.0039
[70] Z.Y. Hu, Z.H. Zhang, X.W. Cheng, F.C. Wang, Y.F. Zhang, S.L. Li, A review of multi-physical fields induced phenomena and effects in spark plasma sintering: Fundamentals and applications, Mater. Des. 191 (2020) 108662, https://doi.org/10.1016/j.matdes.2020.108662
[71] C. Morin, S. Le Gallet, M. Ariane, F. Bernard, Spark Plasma Sintering tool design for preparing alumina-based Functionally Graded Materials, Ceram. Int. 42 (2016) 3056–3063, https://doi.org/10.1016/j.ceramint.2015.10.092